BIOCHEMISTRY
including biophysical chemistry & molecular biology

Article

pubs.acs.org/biochemistry

Examining the Role of Intersubunit Contacts in Catalysis by 3-Deoxy-D-*manno*-octulosonate 8-Phosphate Synthase

Timothy M. Allison,[§] Fiona C. Cochrane,[†] Geoffrey B. Jameson,[†] and Emily J. Parker*[,§]

[†]Institute of Fundamental Sciences, Massey University, Palmerston North, New Zealand

[§]Biomolecular Interaction Centre and Department of Chemistry, University of Canterbury, Christchurch, New Zealand

Supporting Information

ABSTRACT: 3-Deoxy-D-*manno*-octulosonate 8-phosphate synthase (KDO8PS) catalyzes the reaction between phosphoenolpyruvate and arabinose 5-phosphate (A5P) in the first committed step in the pathway to 3-deoxy-D-*manno*-octulosonate, a component in the cell wall of Gram-negative bacteria. KDO8PS is evolutionarily and structurally related to the first enzyme of the shikimate pathway, 3-deoxy-D-*arabino*-heptulosonate 7-phosphate synthase (DAH7PS), which uses erythrose 4-phosphate in place of A5P. Both KDO8PS and type Iβ DAH7PS enzymes adopt similar homotetrameric associations with their active sites close to one of the interfaces. The conserved PAFLxR motif in KDO8PS and the corresponding GARNxQ motif in type Iβ DAH7PS, both on the short β4-α4 loop of the $(\beta/\alpha)_8$ barrel, form part of this interface and provide key contacts with substrates. This ^{112}PAFLxR^{117} motif was mutated in *Neisseria meningitidis* KDO8PS in order to assess its role in enzyme function. Arg117 extends across the interface to provide guanidinium functionality in the A5P binding site of the adjacent subunit. Substitution Arg117Ala severely hampered catalysis, whereas substitution to Lys was tolerated better. Mutation of Phe114 to either Arg or Ala results in active proteins, but with substantially elevated K_m^{A5P} values. Mutant proteins that combine substitutions in this motif demonstrate poor catalytic function, and, although these mutated residues now structurally resemble their counterparts in the GARNxQ motif of type Iβ DAH7PS, no DAH7PS-like activity was observed. Analysis of the structures reveals that small changes in relative orientation of the subunits are important for the differences in active-site construction. Quaternary structure is therefore tightly linked to substrate specificity.

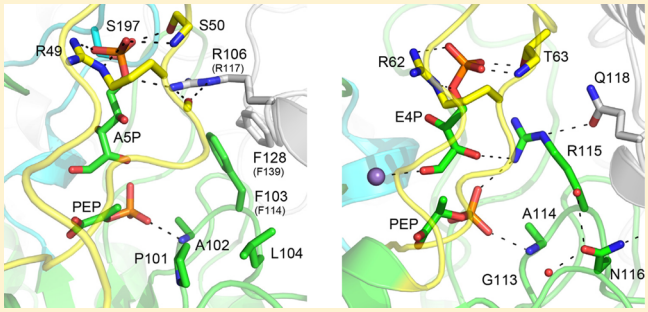

The enzyme 3-deoxy-D-*manno*-octulosonate 8-phosphate (KDO8P) synthase (KDO8PS, EC 2.5.1.55) catalyzes the reaction between phosphoenolpyruvate (PEP) and D-arabinose 5-phosphate (A5P), to produce KDO8P. This reaction is the first step in the biosynthesis of 3-deoxy-D-*manno*-octulosonate, which is an essential component in the lipopolysaccharide layer of Gram-negative bacteria (Figure 1). KDO8PS is mechanistically, structurally, and evolutionarily related to 3-deoxy-D-*arabino*-heptulosonate 7-phosphate synthase (DAH7PS, EC 2.5.1.54).[1,2] DAH7PS catalyzes the coupling of D-erythrose 4-phosphate (E4P) to PEP.[1,3,4] This reaction is the first step of the shikimate pathway for the biosynthesis of aromatic compounds in plants and microorganisms (Figure 1).[5]

KDO8PSs have been isolated and studied from a variety of sources including *Escherichia coli*, *Neisseria meningitidis*, *Aquifex aeolicus*, *Salmonella typhimurium*, *Aquifex pyrophilus*, *Helicobacter pylori*, *Arabidopsis thaliana*, and *Neisseria gonorrheae*.[3,6−14] Some KDO8PSs require a divalent metal ion for catalysis, whereas others do not, and these metal-dependent and metal-independent forms can be readily interconverted by mutation around the metal binding site.[2,6,15−18] The monomeric structure of KDO8PS features the common $(\beta/\alpha)_8$ triose phosphate isomerase (TIM)-barrel fold, enhanced by extensions to the $\beta-\alpha$ loops that extend from the C-terminal end of the barrel and form the active site of the enzyme (Figure 2A).[8] In solution and crystal form the 30 kDa monomers form homotetramers (Figure 2B). This tetrameric quaternary assembly is the functional form of the enzyme, with each monomeric subunit containing an active site. PEP binding is achieved by interactions with residues close to the ends of the β-strands of the core barrel. Three long loops (β2-α2, β7-α7, β8-α8), which link the ends of the β-strands and corresponding α-helices and extend from the barrel, create the A5P binding site and support intersubunit contacts in the tetrameric protein.[8]

In contrast to the KDO8PSs, the structures of the DAH7PSs are more variable.[19] Although both enzymes share the common catalytic barrel, DAH7PSs have barrel extensions and quaternary structure variations that are associated with allosteric regulation of this enzyme by aromatic end products.[9,20−22] DAH7PSs have been divided into a number of families, and KDO8PSs appear to be most closely related to the type Iβ group of DAH7PSs. KDO8PS and type Iβ DAH7PSs share the highest sequence identity (~30%) and have been shown to adopt similar tetrameric quaternary structures.[6,8,23] The type Iβ DAH7PSs

Received: April 26, 2013
Revised: June 1, 2013
Published: June 7, 2013

   dx.doi.org/10.1021/bi400521f | *Biochemistry* 2013, 52, 4676−4686

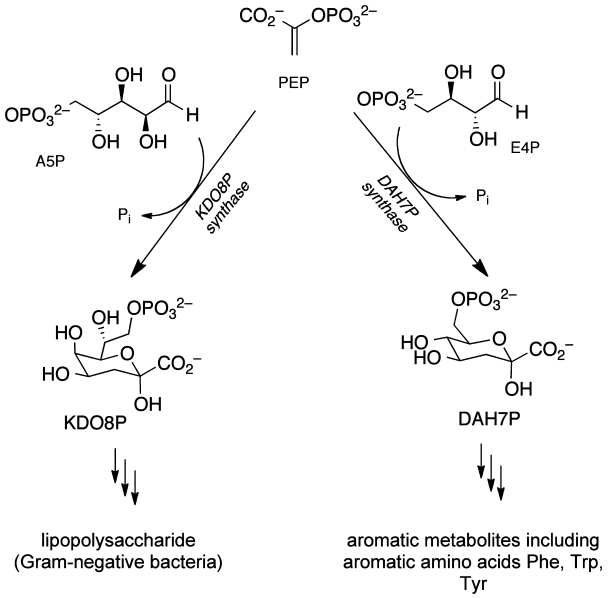

Figure 1. Reactions catalyzed by KDO8PS and DAH7PS.

include the structurally characterized *Pyrococcus furiosus* and *Aeropyrum pernix* DAH7PSs (*Pfu*DAH7PS and *Ape*DAH7PS), which show the greatest overall similarity to the KDO8PS enzymes.[24,25] The active site of DAH7PS comprises two long loops (β2-α2 and β8-α8); the extended β7-α7 loop of KDO8PS is not a structural feature of DAH7PS. Notwithstanding different quaternary associations, and these loop variations, KDO8PS and DAH7PS enzymes have in common many active-site residues located in structurally similar positions.

Although each subunit of the homotetrameric KDO8PS possesses a discrete active site, quaternary associations mean that adjacent active sites within the dimeric unit are closely positioned. There is a conserved sequence motif within the interface area between the two closely juxtaposed active sites that may play a key role in the interaction between the active sites. Specifically, the PAFLxR motif of the relatively short β4-α4 loop contributes both to the PEP binding and directly to substrate binding in the neighboring active site (Figure 3A). The Pro residue of this motif appears to mediate a bend at the top of the β4 strand at the beginning of the loop, while the Phe residue interacts across the interface with a conserved Phe on the β5-α5 loop from the adjacent monomer. A notable feature of the motif is the Arg residue, which interdigitates across the interface into the active site of the adjacent monomer and contributes to the binding of the phosphate moiety of A5P, and for the metal ion-dependent KDO8PS from *A. aeolicus*[26] this Arg residue may also have a role to play in closure of the β7-α7 loop over the active site. Despite the similarities between the structures of KDO8PS and the related Iβ DAH7PS, and the similar relative placing of the active sites in the tetrameric protein, the PAFLxR motif is not found in DAH7PSs. In its place is a conserved motif composed of the residues GARNxQ (Supporting Information, Figure S1). The Arg, which replaces the Phe of KDO8PS, has hydrogen-bonding interactions with the phosphate moiety of PEP and with the C2 hydroxyl group of E4P (Figure 3B). This Arg is able to form hydrogen-bonding interactions with the phosphate group of E4P, especially when E4P moves deeper into the binding pocket on coupling with the tightly held PEP. Such an interaction is implied by the binding of sulfate in the E4P binding site of the DAH7PS from *Mycobacterium tuberculosis*.[27] Hence in DAH7PS intramolecular interactions by the Arg of the GARNxQ motif appear to replace the intermolecular contacts provided by the Arg residue of the PAFLxR motif. The Gln of DAH7PS, which replaces this interdigitating Arg of KDO8PS, appears to buttress the Arg of the motif into position. These residues may therefore be important in determining selection of the aldehydic substrate.

Previously, the roles of other conserved motifs or residues on the active-site loops of KDO8PS have been explored.[28,29] The KANRS motif on the β2-α2 loop controls the strict A5P substrate configurational requirements of KDO8PS, whereas for DAH7PS the corresponding conserved motif controlling E4P binding is KPR(S/T). The long β7-α7 loop of KDO8PS was also found to be essential for efficient catalysis, and the β8-α8 loop, which houses the two conserved carboxylate residues that in metal-ion dependent KDO8PS form part of the metal-ion binding site, has also previously been investigated and shown to be important for arranging the active site to promote productive substrate binding.[26]

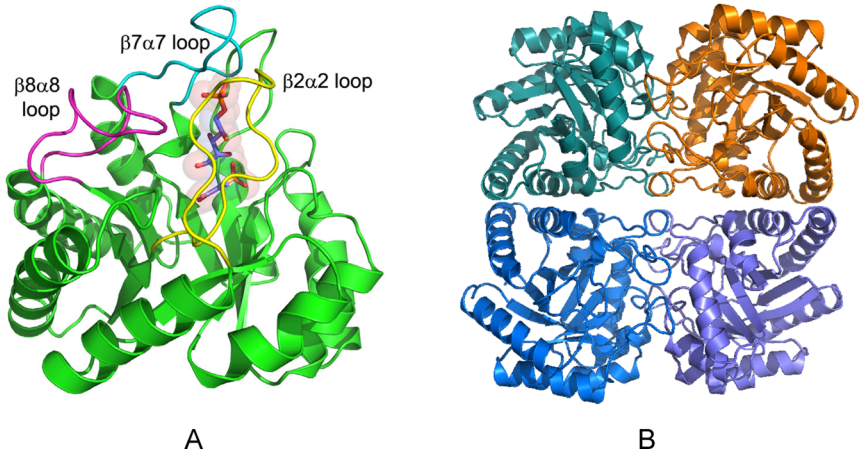

Figure 2. Structure of *Aquifex aeolicus* KDO8PS (PDB code 2NX3). (a) A single monomer of KDO8PS showing the loops that extend the core barrel and the location of the two substrates within the active site. The β2-α2 loop is yellow, β7-α7 loop cyan, and β8-α8 loop magenta. PEP and A5P are shown as both sticks and spheres with carbon atoms colored purple. (b) The homotetramer of KDO8PS. Each monomer is uniquely colored.

dx.doi.org/10.1021/bi400521f | *Biochemistry* 2013, 52, 4676−4686

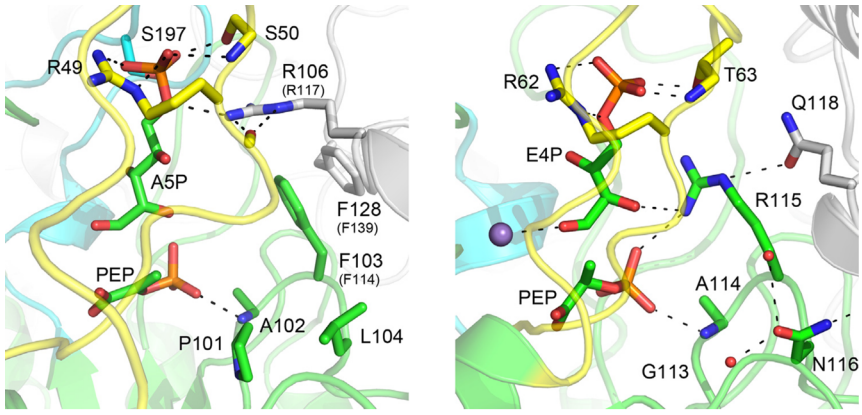

Figure 3. (a) Structure of *Aquifex aeolicus* KDO8PS (PDB code 2NX3) showing the location of the PAFLxR motif on the β4-α4 loop (colored green). The equivalent residue numbers in *Nme*KDO8PS are given in parentheses for residues mutated in this study. (b) Structure of *Pfu*DAH7PS (PDB code 1ZCO, E4P modeled) showing the location of the corresponding GARNxQ motif (colored green). The adjacent monomer is colored white, the β2-α2 loop yellow, and the β7-α7 loop cyan.

Herein, we report a detailed investigation of the role of the PAFLxR motif, using the well-characterized metal-independent KDO8PS from *N. meningitidis* (*Nme*KDO8PS). Our studies on a series of protein variants bearing amino-acid substitutions in this motif show that, while the identity of the residues of this motif are important for efficient catalysis, some variation in this conserved motif can be tolerated for KDO8PS activity.

EXPERIMENTAL PROCEDURES

Bacterial Strains, Plasmids, Media, and Growth Conditions. The wild-type and mutant proteins were expressed with methods similar to those already described.[6,30] Briefly, *E. coli* BL21 (DE3) (Star) cells carrying plasmids encoding the genes for each protein under control of a T7-promoter were grown to OD_{600} = 0.4−0.8 at 37 °C. At this point expression was induced by adding IPTG to a final concentration of 0.5 mM or 1 mM. Cells were either harvested four hours postinduction, or immediately transferred after induction to 23 °C and harvested the following morning (~16 h).

Mutants of the plasmid containing *Nme*KDO8PS were generated using a QuikChange II Site-Directed Mutagenesis Kit (Stratagene), or a Quikchange II Lightning Site-Directed Mutagenesis Kit (Stratagene). Using the pT7−7-*Nme*KDO8PS plasmid as the template (or that already containing other desired mutations), mutant DNA was generated (primer sequences are listed in Table S1).

Enzyme Purification and Assays. All enzymes were purified as previously described using anion-exchange and hydrophobic-interaction chromatography, followed by size-exclusion chromatography.[6,30] The elution profile from the size-exclusion column was similar for all mutant proteins and to wild-type *Nme*KDO8PS. The kinetic assay system used was the same as previously described, based on the rate of consumption of PEP (ε = 2.8 × 10^3 M^{-1} cm^{-1}) measured by the loss of absorbance at 232 nm.

The assays for determining the Michaelis−Menten kinetic parameters kept the concentration of one substrate constant, while varying that of the other and vice versa. To determine K_m^{A5P} for *Nme*R117Q, the concentration of A5P was varied between 111 μM and 5560 μM while the PEP concentration remained constant at 100 μM. To determine K_m^{PEP} for *Nme*F139G, PEP was varied between 7.8 μM and 156 μM with A5P at 1 mM, and for K_m^{A5P}, the concentration of A5P was varied between 39.5 μM and 1580 μM while PEP was held at a concentration of 150 μM. To determine K_m^{A5P} for *Nme*F114R/R117A the concentration of A5P was varied between 133 μM and 3330 μM while the concentration of PEP remained constant at 100 μM, and for *Nme*F114R/R117Q the concentration of A5P was varied between 172 μM and 2580 μM while the concentration of PEP was also held at 100 μM. To determine K_m^{A5P} for *Nme*F114R/R117Q/F139G the A5P concentration was varied between 133 μM and 2931 μM while PEP was held at 100 μM. Assays to determine the activity of *Nme*F114R/R117A, *Nme*F114R/R117Q, and *Nme*F114R/R117Q/F139G with 2-deoxy-D-ribose-5-phosphate, D-ribose 5-phosphate (R5P), and E4P used 1 mM of the aldose substrate and 100 μM of PEP.

Differential Scanning Fluorimetry. The melting temperatures of *Nme*KDO8PS mutants were determined by differential scanning fluorimetry (DSF) using an iCycler iQ5 Multicolor Real-Time PCR Detection System (Bio-Rad). The method used was based on that of Nordlund et al.[31] Triplicate protein samples were added with mixing to buffer (containing additives) and SYPRO orange dye in a 96-well microplate, which was then sealed. The melt proceeded in 0.2 °C increments from 20 to 95 °C, with a 20 s dwell time after each temperature rise. Measurements of the fluorescence were made at the end of each dwell time. The melt temperatures were calculated as the temperature at the point of inflection (maximum slope) of the melting curve after subtracting the reading of a blank well containing buffer and dye but lacking protein.

Crystallization. Crystals of the *Nme*KDO8PS mutants were grown by hanging-drop vapor diffusion. Protein solution (20 mg mL^{-1}, in 10 mM BTP pH 7.5) of each mutant was mixed 1:1 (v/v) with reservoir solution containing 100 mM sodium acetate (pH 4.6) and 0.6−3.0 M NaCl. The drop sizes were 2 μL and the reservoir solution 500 μL. The crystallization trays were left at 20 °C until immediately before data collection, with crystals being transferred briefly into a cryoprotectant composed of 20% glycerol in the respective reservoir solution. Crystals typically began to form after four hours, and were fully formed in 24 h.

Structure Determination and Refinement. A Rigaku MicroMax007 microfocus copper rotating-anode generator with AXCo PX70 focusing capillary optic (λ = 1.5418 Å)

dx.doi.org/10.1021/bi400521f | *Biochemistry* 2013, 52, 4676−4686

Table 1. Crystal Parameters, Data Collection, and Refinement Statistics

	F114A	F114R	F114R/R117A	F114R/R117Q	F114R/R117Q/F139G	R117K	R117Q	F139G
A. Data collection								
Crystal system; space group	$P2_12_12_1$	$P2_12_12_1$	$P2_12_12_1$	$P2_12_12_1$	$P2_12_12_1$	$P2_12_12_1$	$P2_12_12_1$	$P2_12_12_1$
Unit cell parameters (Å) *a, b, c*	81.36, 85.47, 163.06	81.86, 85.20, 163.36	81.59, 85.37, 163.35	82.15, 85.99, 163.11	81.67, 85.20, 162.85	81.47, 85.37, 163.02	81.47, 85.42, 162.71	82.00, 85.92, 163.37
Resolution range (Å)	39.95−1.90 (1.97−1.90)	39.70−1.80 (1.86−1.80)	34.32−1.85 (1.95−1.85)	48.00−2.00 (2.11−2.00)	41.20−1.75 (1.84−1.75)	39.93−1.75 (1.81−1.75)	45.79−1.86 (1.96−1.86)	38.06−2.10 (2.18−2.10)
Measurements	414454	440726	706400	562713	822735	462344	675001	195294
Unique reflections	88194	105281	95642	78806	115042	113642	95950	62633
Redundancy	4.7 (4.4)	4.2 (3.3)	7.4 (7.1)	7.1 (7.3)	7.2 (7.3)	4.1 (2.4)	7.0 (7.2)	3.1 (3.1)
Completeness (%)	97.8 (87.0)	98.7 (93.4)	97.9 (96.8)	100 (100)	100 (100)	98.8 (93.0)	99.9 (100)	92.0 (99.9)
$I/\sigma(I)$	8.8 (1.2)	12.6 (3.2)	9.7 (1.9)	4.1 (2.0)	4.5 (1.8)	14.1 (2.7)	5.1 (1.9)	7.2 (2.3)
R_{merge}	0.065 (0.601)	0.044 (0.302)	0.066 (0.412)	0.115 (0.377)	0.088 (0.419)	0.041 (0.325)	0.090 (0.398)	0.080 (0.395)
Wilson *B*-value (Å^2)	38.3	31.8	20.5	21.5	21.4	32.2	23.5	33.7
B. Refinement								
Resolution (Å)	39.98−1.90 (1.95−1.91)	39.74−1.80 (1.85−1.80)	33.58−1.85 (1.90−1.85)	45.93−2.00 (2.05−2.00)	40.82−1.75 (1.80−1.75)	39.55−1.75 (1.79−1.75)	41.31−1.86 (1.91−1.86)	37.09−2.10 (2.15−2.10)
R_{cryst}	0.22860	0.18461	0.16094	0.15902	0.15900	0.19647	0.17628	0.21698
R_{free}	0.26692	0.21498	0.19087	0.19444	0.18844	0.22633	0.20633	0.24986
Chain length	280	280	280	280	280	280	280	280
Observed number of residues (chain A, B, C, D)	276, 277, 277, 276	277, 279, 277, 277	277, 278, 278, 277	277, 278, 277, 277	277, 279, 277, 277	277, 279, 278, 277	277, 279, 278, 277	277, 279, 277, 277
Water molecules	324	452	790	795	716	338	505	130
Other	2 × Cl^-, 1 × Na^+	6 × Cl^-, 1 × Na^+, 2 × Glycerol	6 × Cl^-, 1 × Na^+, 1 × Glycerol	5 × Cl^-, 1 × Na^+, 1 × Glycerol	5 × Cl^-	3 × Cl^-, 1 × Na^+	4 × Cl^-, 1 × Na^+	2 × Cl^-
Mean *B* (Å^2)								
Protein	47.05	33.84	26.60	27.51	28.01	36.02	30.69	40.64
Water	41.28	35.83	32.43	34.33	34.94	33.80	31.84	30.50
Other	59.50	34.81	31.61	40.00	31.75	31.75	31.75	31.75
r.m.s.d. from target values								
Bond lengths (Å)	0.017	0.019	0.020	0.019	0.021	0.018	0.019	0.016
Bond angles (°)	1.757	1.816	1.895	1.820	1.959	1.797	1.817	1.709
Dihedral angles (°)	5.588	5.679	5.882	5.750	5.827	5.700	5.671	5.919
Ramachandran								
Preferred (%)	97.46	97.34	97.75	97.02	97.87	97.76	97.45	97.35
Allowed (%)	1.93	2.25	1.71	2.45	1.52	1.83	2.04	2.04
Outliers (%)	0.61	0.41	0.54	0.53	0.61	0.41	0.51	0.61
PDB entry	4JTE	4JTF	4JTG	4JTH	4JTI	4JTJ	4JTK	4JTL

dx.doi.org/10.1021/bi400521f | *Biochemistry* 2013, 52, 4676−4686

coupled with an RAxisIV^{++} image-plate detector was used to collect data sets at 120 K (Oxford Cryosystems Series 700) for *Nme*F139G, *Nme*F114A, *Nme*F114R, and *Nme*R117K. Data collection and processing were performed with CrystalClear.[32]

Data sets for the other proteins were collected at the Australian Synchrotron using the MX2 beamline (for *Nme*F114R, *Nme*R117Q, *Nme*F114R/R117Q, and *Nme*F114R/R117Q/F139G) or the MX1 beamline (for *Nme*F114R/R117A) and were processed using iMosFlm and SCALA (CCP4 suite[33]). The results are summarized in Table 1, along with key structure-refinement details. Data were collected for crystals of *Nme*F139G grown in a 0.6 M NaCl condition, *Nme*F114R in 0.6 to 2.8 M NaCl, *Nme*R117Q in 1.4 M NaCl, *Nme*F114R/R117Q in 0.6 to 2.8 M NaCl, *Nme*F114R/R117Q/F139G in 2 M NaCl, and *Nme*F114R/R117A in 1.6 M NaCl. All mutant proteins crystallize like wild-type in the orthorhombic space group $P2_12_12_1$ with unit cell dimensions $a \approx 82$ Å, $b \approx 85$ Å, and $c \approx 163$ Å. The wild-type *Nme*KDO8PS structure was used to solve the structure of the mutants, carrying through the same set of reflections for calculation of R_{free}. Refinements were carried out with Refmac5,[34] and electron density maps were analyzed with COOT.[35] Molprobity and the validation tools of COOT were used to check for, and correct, conformational infelicities. All diagrams were drawn with PyMol.

RESULTS

Choice of Mutant Constructs. The conserved PAFLxR motif in KDO8PS and the corresponding GARNxQ motif in DAH7PS, both on the short $\beta4$-$\alpha4$ loop, form part of the interface between subunits and also provide key contacts with the PEP and A5P (and, for DAH7PS, with E4P) substrates. In particular, the Phe and Arg residues of the PAFLxR motif and the Arg and Gln residues of the GARNxQ motif form key interface contacts. Accordingly, selected mutations to the ^{112}PAFLxR^{117} motif in *Nme*KDO8PS were created by site-directed mutagenesis (Table 2) in order to probe the roles of these conserved residues on the stability, kinetics, substrate selection, and structure of *Nme*KDO8PS. Phe114 of the motif was mutated separately to Ala and Arg, creating *Nme*F114A and *Nme*F114R. The conserved Phe139, which is not part of the motif but with which Phe114 partners by π interactions, was mutated to Gly (creating *Nme*F139G); Gly is the conserved identity of the equivalent residue in the type Iβ DAH7PSs. The Arg, which interdigitates into the active site of the adjacent monomer, was mutated to (i) Ala (creating *Nme*R117A), (ii) Gln (as found in DAH7PS) creating *Nme*R117Q, and (iii) Lys creating *Nme*R117K. Variants of *Nme*KDO8PS that contained combinations of these mutations were also created: *Nme*F114R/R117A, *Nme*F114R/R117Q, and *Nme*F114R/R117Q/F139G. The latter two resemble the pairings of residues found in the GARNxQ motif of DAH7PS. The combination of F114R and R117Q both replaces the interdigiting Arg residue of KDO8PS with an intramolecular active-site Arg as found in DAH7PS and provides the intermolecular buttressing that may be important in correctly postioning this residue (Figure 3B).

The mutant proteins were purified using the same procedures as those developed for the purification of wild-type *Nme*KDO8PS and the melting temperatures of the proteins were measured by DSF (Table S2, Supporting Information).

The mutated proteins were found to vary in stability relative to the wild-type *Nme*KDO8PS (Table S2, Supporting Information), both intrinsically and in the presence of additives, especially Cd^{2+}, which has a large destabilizing effect for wild-type *Nme*KDO8PS.[6] Variant *Nme*F114A was generally more stable than wild-type protein in all conditions (by 6 to 8 °C), and interestingly, the T_m value was not affected by the presence of Cd^{2+}. Although *Nme*F139G had similar T_m values to wild-type *Nme*KDO8PS in all conditions, like *Nme*F114A, the T_m value was also not affected by the presence of Cd^{2+}. In contrast, *Nme*F114R was generally less stable than wild-type *Nme*KDO8PS (by 3 to 5 °C), and the presence of Cd^{2+} destabilized this mutant further. The *Nme*R117Q protein was generally more stable than wild-type *Nme*KDO8PS (by 11 to 12 °C), but only showed a slight destabilization in the presence of Cd^{2+}. The melt temperatures for both double mutants (*Nme*F114R/R117A and *Nme*F114R/R117Q) and the triple mutant (*Nme*F114R/R117Q/F139G) were similar to those for wild-type *Nme*KDO8PS. Moreover, these mutants showed a destabilization in the presence of Cd^{2+} similar to that of wild-type *Nme*KDO8PS. Mutants in which the location of the Arg was swapped (*Nme*F114R/R117A, *Nme*F114R/R117Q, and *Nme*F114R/R117Q/F139G) were all markedly stabilized by 7−8 °C by the addition of PEP.

Table 2. Mutations of *Nme*KDO8PS

Construct	Mutation location	Reason
F114A	PA**F**LxR	Probe intersubunit π interactions
F114R	PA**F**LxR	Conversion to residue in DAH7PS
R117A	PAFLx**R**	Probe role of charge on Arg
R117K	PAFLx**R**	Probe importance of Arg
R117Q	PAFLx**R**	Conversion to residue in DAH7PS
F139G	$\beta5$-$\alpha5$ loop	Conversion to residue in DAH7PS
F114R/R117A	PA**F**Lx**R**	Partial conversion to residues of DAH7PS
F114R/R117Q	PA**F**Lx**R**	Conversion to residues in DAH7PS
F114R/R117Q/F139G	PA**F**Lx**R** and $\beta5$-$\alpha5$ loop	Conversion to residues in DAH7PS

Kinetic Properties of the Altered Proteins. The enzyme activities and kinetic parameters for the mutant enzymes were measured (Table 3). The mutation F139G had no negative effect on the reaction rate; in fact, the value of k_{cat} for *Nme*F139G was slightly higher than that for wild-type *Nme*KDO8PS. Residue Phe139 is in the interface area between adjacent monomers and has no direct interactions with the active-site residues of either its own subunit or that of the adjacent one (Figure 3A). However, K_m^{A5P} for this enzyme is raised by nearly fifty-fold relative to wild-type enzyme, which suggests that this residue has a significant role to play in promoting the binding of A5P to the enzyme. The same effect on K_m^{A5P} was observed for *Nme*F114A, and there was a slight decrease in the value of k_{cat} for this enzyme. The mutation of Phe to Arg, which is the corresponding residue in DAH7PS, was detrimental to the binding of PEP, but was less detrimental to the binding of A5P, although K_m^{A5P} for *Nme*F114R is substantially increased to more than 20 times that for wild-type enzyme.

Mutation of the interdigitating Arg to Lys (*Nme*R117K) slightly reduced the value of k_{cat}, but substantially disrupted the binding of A5P, observed by a large increase in the value of K_m^{A5P}. The introduced Lys residue may partially fulfill the role of the native Arg residue, as, in contrast, the mutation to Ala was highly disruptive to enzyme activity, with this enzyme (*Nme*R117A) being barely active. Mutation to Gln, which is the residue found in this position in DAH7PS, resulted in a protein with a very large K_m^{A5P} value, but which was still moderately

dx.doi.org/10.1021/bi400521f | *Biochemistry* 2013, 52, 4676−4686

active, with the value of k_{cat} reduced to an eighth of that for wild-type *Nme*KDO8PS. These results collectively suggest that the interdigitating Arg117 is important for the binding of A5P to the enzyme.

The double and triple mutant proteins, all of which include mutation of Arg117, have dramatically increased K_m^{A5P} values. The k_{cat} values for these three enzymes were also much lower than for enzymes containing any of the single mutations alone (except for *Nme*R117A, which was essentially inactive). Interestingly, coupling the mutation F114R with R117A restored a small amount of activity compared to the devastating effect of the single R117A mutation. This shows that the complete loss of the Arg side chain could be tolerated by adding functionality with the Phe114 substitution. All of the double and triple mutant protein variants were tested with A5P alternatives, 2-deoxyribose 5-phosphate and ribose 5-phosphate and the DAH7PS substrate D-erythrose 4-phosphate. No loss of PEP was detected in the presence of any of these alternative substrates; in other words, none is a substrate.

Structures of *Nme*KDO8PS Variants. Crystals were grown and diffraction data collected for eight mutants of *Nme*KDO8PS: F114A, F114R, R117Q, R117K, F139G, F114R/R117A, F114R/R117Q, and F114R/R117Q/F139G. As for wild-type *Nme*KDO8PS, the asymmetric unit for each structure contains one complete tetramer. Generally the models for each structure were very similar to that of the wild-type protein and to each other, apart from the differences at the substituted residues, and some local collateral damage due to the substitutions.

F114A and F114R. In the structure of *Nme*F114A, there are no major differences in the structure apart from the truncation of the side chain at position 114 caused by the mutation to Ala (RMSD of Cα atoms on the superimposed wild-type structure of 0.330 Å).

In the structure of *Nme*F114R the side chains of F114R in all subunits are more disordered with density only resolved to the Cβ atom in chains A and C. Other than the poorly defined electron density for the side chains of F114R, there is one other notable change to the structure. For the first time ever in a structure of *Nme*KDO8PS, a fully ordered $\beta7$-$\alpha7$ loop is observed (in chain B only). The full $\beta7$-$\alpha7$ loop has only ever been observed before in structures of *Aae*KDO8PS (an enzyme from a hyperthermophilic source) in which both PEP and A5P (or the reaction intermediate or product) are bound.[8,15] In this structure of *Nme*F114R the $\beta7$-$\alpha7$ loop appears in a different conformation to that observed in *Aae*KDO8PS (Figure 4), representing the conformational flexibility in this dynamic and mobile loop.[28] The conserved Gln (Gln202) at the bottom of the loop is in clearly defined density, and positioned pointing in toward the active site, in a similar orientation to that observed in structures of *Aae*KDO8PS.

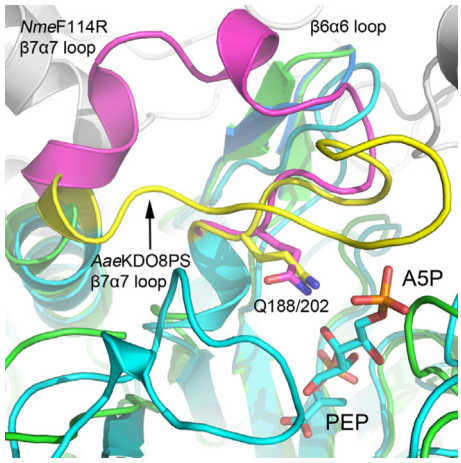

Figure 4. Structure of *Nme*F114R (green) with that of *Aae*KDO8PS (PDB code 2NX3) superimposed (cyan). The $\beta7$-$\alpha7$ loop in *Nme*F114R is colored magenta, and in *Aae*KDO8PS is colored yellow. The top of the $\beta6$-$\alpha6$ loop has shifted in the structure of *Nme*F114R; that of wild-type *Nme*KDO8PS is shown in cartoon and colored blue. The other subunits of the *Nme*F114R tetramer are colored white.

R117Q and R117K. The structure of *Nme*R117Q, where the interdigitating Arg residue, which extends across the subunit interface into the neighboring active site, is replaced by the Gln present in Iβ DAH7PS, as with the other structures, shows no changes relative to the wild-type protein other than that for the substituted amino acid. In all chains the Gln occupies a similar position to the Arg in wild-type *Nme*KDO8PS (Figure S2A, Supporting Information), although in chains B−D the residue is poorly ordered. When Arg117 is mutated to Lys, the mutation appears to have induced no other changes in structure, as observed in the model of *Nme*R117K. The Lys side chain occupies the same position as Arg in wild-type *Nme*KDO8PS (Figure S2A, Supporting Information).

F139G. Mutation of Phe139 to Gly (as found in type Iβ DAH7PS) has no effect on the observed conformation of Phe114, the residue with which the native Phe residue interacts across the subunit interface. However, the structure of *Nme*F139G reveals that the interdigitating Arg (Arg117) has shifted toward the void created by the mutation in chains B and C (Figure S2B, Supporting Information). In chain A, Arg117 is disordered and in chain D it occupies a similar position as in

Table 3. Kinetic Parameters Determined for *Nme*KDO8PS Variants[a]

KDO8PS	K_m^{PEP} (μM)	K_m^{A5P} (μM)	k_{cat} (s^{-1})	k_{cat}/K_m^{A5P} (s^{-1} mM^{-1})
*Nme*WT	2.5 ± 0.2	12.0 ± 0.5	8.0 ± 0.1	660 ± 40
*Nme*F139G	14 ± 1	594 ± 30	8.6 ± 0.2	14 ± 1
*Nme*F114A	58 ± 6	873 ± 29	6.1 ± 0.2	7.0 ± 0.5
*Nme*F114R	95 ± 7	285 ± 18	3.0 ± 0.1	11 ± 1
*Nme*F114R/R117A	ND	3700 ± 400	0.108 ± 0.007	0.029 ± 0.005
*Nme*F114R/R117Q	ND	2742 ± 173	0.27 ± 0.01	0.10 ± 0.01
*Nme*F114R/R117Q/F139G	ND	3600 ± 400	0.14 ± 0.01	0.039 ± 0.007
*Nme*R117K	22 ± 1	816 ± 32	4.8 ± 0.1	5.9 ± 0.4
*Nme*R117A	ND	ND	~0.01	ND
*Nme*R117Q	ND	3211 ± 196	1.06 ± 0.03	0.33 ± 0.03

[a]The K_m^{PEP} values were not determined (ND) for some mutant variants due to the very low enzyme activity.

dx.doi.org/10.1021/bi400521f | *Biochemistry* 2013, 52, 4676−4686

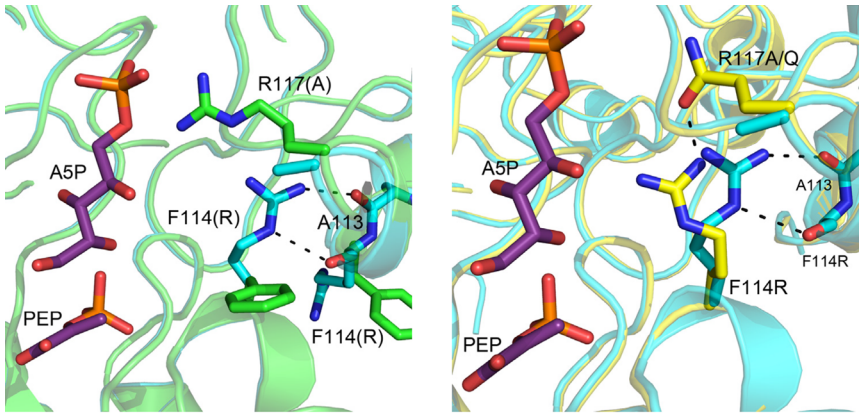

Figure 5. (a) Structure of *Nme*F114R/R117A (cyan) superimposed with that of wild-type *Nme*KDO8PS (green, PDB code 2QKF). PEP and A5P (carbon atoms colored magenta) are from the superimposed structure of *Aae*KDO8PS (PDB code 2NX3). (b) Structure of *Nme*F114R/R117Q (yellow) superimposed onto that of *Nme*F114R/R117A (cyan). PEP and A5P (carbon atoms colored magenta) are from the superimposed structure of *Aae*KDO8PS (PDB code 2NX3).

wild-type *Nme*KDO8PS. The increased mobility of Arg117 in this model of *Nme*F139G correlates with the increase in K_m^{A5P} for this enzyme.

F114R/R117A. In contrast to the structure of *Nme*F114R, where the Arg side chain was generally disordered, in the structure of the double mutant *Nme*F114R/R117A the side chain of F114R is well-ordered. In chains A and B, NE and NH2 of F114R hydrogen bond with the main-chain carbonyl atoms of F114R and Ala113, respectively, from the adjacent subunit (Figure 5A). Generally, in all chains, the side chain of F114R is close to encroaching upon the position occupied by Arg117 in structures of wild-type *Nme*KDO8PS. Hence, the truncation of Arg117 to Ala appears to have allowed room for a more favorable and ordered positioning of the side chain of F114R. However, the conformation F114R adopts in this structure is not that observed in structures of type Iβ DAH7PSs, and thus it is not ideally positioned in this conformation to interact with the phosphate moiety of PEP, or the C2-OH of A5P or E4P.

F114R/R117Q and F114R/R117Q/F139G. In the structure of *Nme*F114R/R117Q the introduced Gln residue does appear to buttress F114R, pushing it further in toward the active site (Figure 5B). In all four chains, the side chain of F114R hydrogen bonds with R117Q and is closer in position to that of the equivalent Arg in type Iβ DAH7PSs. In the structure of *Nme*F114R/R117Q/F139G the introduction of F139G has led to an increase in the range of conformations sampled by F114R. In chains A and D, F114R is in the same conformation as observed in the structure of *Nme*F114R/R117Q, and in chain B, F114R adopts a similar position to that observed in the structure of *Nme*F114R/R117A. In chain C the side chain of F114R is disordered.

DISCUSSION

Residues of a conserved motif that contribute to the active site, and which are located in the interface area between adjacent monomers in KDO8PS, were mutated to assess their role in substrate binding. The mutant proteins behaved similarly to wild-type *Nme*KDO8PS in that they were able to be purified and crystallized using the same protocols, notwithstanding changes in protein charge that accompanied several of the mutations. The melt temperatures measured for the proteins varied, with changes relative to wild-type values for most variants consistent with modification to the interface area between subunits. Structural analysis of the variant proteins indicated that the introduced mutations caused only local structural changes primarily associated with the change in side-chain functionality, and generally induced no major changes in structure, especially with respect to the quaternary structure, and the relative positioning of subunits. However, the mutations altered the kinetic parameters of all the variant enzymes, with particular impact on the value of K_m^{A5P} and the turnover number, k_{cat}.

Role of Cd^{2+} in the (In)stability of *Nme*KDO8PS. The curious effect of Cd^{2+}, but not Mn^{2+} or Co^{2+}, on the stability of *Nme*KDO8PS, which does not require a divalent metal ion for activity, has been noted previously.[30] The results obtained on these interface mutants are intriguing to say the least. With the marginal exception of the *Nme*F114R mutant, the greater the stabilization of the mutant enzyme caused by binding PEP, the greater the destabilization caused by the presence of Cd^{2+}. Although not measured here on mutant enzymes, Cd^{2+} also has a profound effect on enzyme activity for *Nme*KDO8PS.[6] We have not so far been able to grow crystals in the presence of Cd^{2+} under conditions that readily produce crystals of *Nme*KDO8PS and its numerous mutants, suggesting that in binding to the enzyme Cd^{2+} triggers a destabilizing change in quaternary structure. We have inspected structures closely for potential Cd^{2+}-binding sites. The conformationally promiscuous Gln118 is in weak contact across the subunit interface with His94; this His is part of a cluster of potential ligands, including Asp92, Ser54, and Asp56, that with minor reorientation could potentially form a metal-binding site.

Part of the interface studied features a close 2.8 Å Glu95-Glu95 contact, where one or another of these Glu carboxylates must be protonated. Uniquely for the F114A mutant, the mutant with enhanced stability relative to wild-type enzyme and not destabilized by the addition of Cd^{2+}, these carboxylate side chains are oriented away from each other and instead make intramolecular hydrogen-bonding contacts. The other mutation that shows substantially enhanced stability relative to wild-type enzyme and suffers only a small destabilization by Cd^{2+} is

dx.doi.org/10.1021/bi400521f | *Biochemistry* 2013, 52, 4676−4686

R117Q. Here, the increased stability is attributed to the removal of positive charge from the interface region coupled with maintenance of interface packing.

Interdigitating Arg Helps Form the A5P Binding Site. The equivalent residue to Arg117 is in *Aae*KDO8PS Arg106. In a previous study the *Aae*KDO8PS mutant R106G was created and the mutation was found to impair closure of the $\beta7$-$\alpha7$ loop.[26] It was suggested that the loss of the Arg residue affected the positioning of the $\beta2$-$\alpha2$ loop, which houses the KANR(S/T) motif that supplies many of the active-site interactions with A5P. It was also suggested that the slight shift in the position of the $\beta2$-$\alpha2$ loop observed in crystal structures of *Aae*R106G (with no substrates bound, with only PEP bound, and with both PEP and A5P bound) negatively impacted the binding of A5P and was associated with the change in ability of the $\beta7$-$\alpha7$ loop to close. For the *Aae*KDO8PS R106G variant, the K_m^{A5P} value increased (from 7 ± 3 μM to 60 ± 20 μM) and the changes in this value were attributed to both the direct loss of the Arg side chain, which hydrogen bonds with the phosphate moiety of A5P, and, indirectly, the changed dynamics of the $\beta7$-$\alpha7$ loop.

The results presented here for *Nme*KDO8PS are largely consistent with this picture and with the role of the Arg to secure the formation of the complete binding site for the A5P phosphate moiety. However, loss of the guanidinium side chain by substitution of the Arg117 (equivalent to Arg106 in *Aae*KDO8PS) by Ala has a far more dramatic effect on the activity of *Nme*KDO8PS. Exchange to Gln (*Nme*R117Q) resulted in a large increase in the value of K_m^{A5P} and significant reduction in k_{cat}, whereas for *Nme*R117K, in which the Lys residue can fulfill some of the same role as the native Arg, the effect on K_m^{A5P}, was more modest, but still larger than that observed for the *Aae*R106G enzyme.

In contrast to the results for *Aae*KDO8PS, mutation of Arg117 in *Nme*KDO8PS appears to have no effect on the positioning of the $\beta2$-$\alpha2$ loop in the structures of all *Nme*KDO8PS proteins in which this Arg was mutated. The differences between the observed effects of mutation of *Nme*KDO8PS and *Aae*KDO8PS may be attributable to differences between the mesophilic (*Nme*KDO8PS) and thermophilic (*Aae*KDO8PS) sources of the two enzymes. Additionally, *Nme*KDO8PS is a metal-independent KDO8PS, while *Aae*KDO8PS is a metal-dependent enzyme. It has been previously demonstrated that the metal-independent active-site scaffold is more susceptible to disruption in substrate binding.[29]

In the *Aae*KDO8PS structures (PDB codes 1FWW and 2NX3), near the bound A5P, Arg106 makes intersubunit contact with the main-chain carbonyl oxygen of the Asn of the KANRS motif, which is responsible for the binding of A5P. There is also a long hydrogen bond across the interface to the Ser of this KANRS motif established in some structures. Arg106 does make direct hydrogen-bonding contact with the bound A5P in the A5P bound metal-independent variant of *Aae*KDO8PS (PDB code 2NX3), and there is also some hydrophobic packing across the subunit interface of the methylene part of the side chain of this Arg against Phe of the PAFLxR motif. For *Nme*KDO8PS, similar hydrophobic packing is observed, but no direct hydrogen-bonding contact is made with loop $\beta2$-$\alpha2$, possibly due to the absence of bound A5P. A key role of this Arg for both *Aae*- and *Nme*KDO8PS seems to be simple electrostatic guidance of the A5P. This is important as the PEP, which binds first, offers strong electrostatic repulsion to the binding of A5P. The importance of this role is reinforced by the nearly inactive R117A mutant, whereas the R117K mutant suffers only an 8-fold drop in k_{cat}.

Subunit Interface Is Important for Substrate Binding. Phe114 was mutated in *Nme*KDO8PS to Ala or Arg, the latter being the conserved identity of this residue in type Iβ DAH7PSs. In the crystal structures of these mutant proteins there are no major changes observed other than in the immediate vicinity of the mutations (other than the unusual ordering of the $\beta7$-$\alpha7$ loop noted for *Nme*F114R). Despite the region surrounding Phe114 normally being well ordered, in the structure of *Nme*F114R the side chain of F114R is largely disordered. An unfavorable entropic factor resulting from the fact that the binding site is not preorganized, as in the wild-type enzyme, to accept substrates may account for why these modifications to F114 have caused a modest increase in the values of K_m^{PEP} and K_m^{A5P} for these enzyme variants. Interestingly, the increase in value of K_m^{A5P} for *Nme*F114R is more modest than for *Nme*F114A compared to wild-type *Nme*KDO8PS. This observation suggests that the catalytic function of KDO8PS is relatively accommodating of an Arg residue at this position, although there might be some loss in protein stability as the melt temperature of *Nme*F114R is 3 to 5 °C less than that for wild-type *Nme*-KDO8PS. Given the similarity between KDO8PS and DAH7PS and the evolutionary origin of KDO8PS from a likely Arg-containing protein, the accommodation of an Arg residue at this position is perhaps not surprising. It has been previously proposed that the presence of this Phe residue for KDO8PS in the vicinity of the PEP's phosphate functionality may correlate to the binding of the dianionic form of PEP (with a single charge on the phosphate group), whereas the Arg found in this position for DAH7PS may be linked to the binding of PEP in the trianionic form.[36] The observation in these studies that the Arg can be relatively easily accommodated without major penalty to catalysis, suggests that this difference is not an important feature for distinguishing KDO8PS function.

In structures of *Pfu*DAH7PS in which PEP is bound and E4P has been modeled, the equivalent Arg residue at residue 114 may interact not only with the phosphate moiety of PEP, but also with C2-OH of E4P (Figure 3B).[24] It is conceivable then that the Arg introduced into *Nme*KDO8PS by the mutation F114R may have a similar, but perhaps not optimized, interaction with C2-OH of A5P (and a potentially better interaction with C2-OH of E4P or R5P, which both have the same but opposite configuration to A5P at this stereogenic center). However, when tested for DAH7PS-like activity, the F114R/R117A, F114R/R117Q, and F114R/R117Q/F139G variant proteins showed no detectable activity with either E4P or R5P.

In contrast to the structure of *Nme*F114R, in the structures of the double and triple mutant proteins, in which the F114R mutation is coupled with mutations of Arg117 and Phe139 (*Nme*F114R/R117A, *Nme*F114R/R117Q, and *Nme*F114R/R117Q/F139G), the side chain of F114R is ordered. Although removal of the interdigitating Arg functionality severely affects the ability of A5P to bind to the enzyme for reasons discussed above, it does begin to allow F114R to be positioned in the active site to more closely resemble the DAH7PS active-site architecture. The conformation of the F114R side chain in structures of *Nme*KDO8PS is not in exactly the same position as in structures of type Iβ DAH7PSs (Figure 6); however, some optimization in position was observed through the buttressing of F114R by R117Q in comparison to the positions

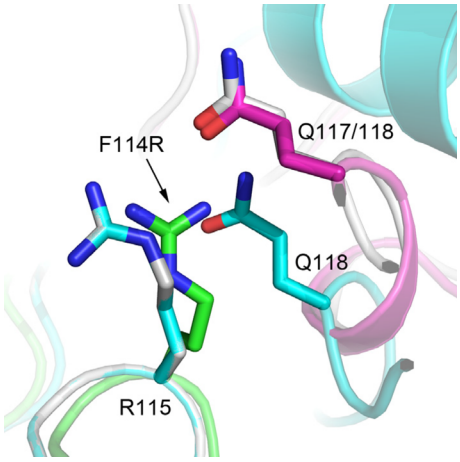

Figure 6. Quaternary structure interactions of *Pfu*DAH7PS (PDB code 1ZCO) compared to the structure of *Nme*F114R/R117Q. Superposition of chain A of the *Pfu*DAH7PS tetramer (colored cyan) onto chain A on *Nme*F114R/R117Q (green), and separately of chain C of *Pfu*DAH7PS (colored white) onto chain C of *Nme*F114R/R117Q (magenta). The actual position of residues at the AC interface is seen by comparing the cyan-colored *Pfu*DAH7PS with the green- and magenta-colored *Nme*F114R/R117Q.

adopted by F114R when coupled with the mutation R117A. The structural changes observed in these multiply substituted variants do not seem to be correlated to significant changes in the kinetic parameters for these proteins, although it is noted that the addition of the F114R mutation to *Nme*R117A does create a protein with detectable catalytic activity.

Quaternary Structure Is Important for Substrate Selectivity. The results in these studies demonstrate that the construction of the subunit interface area, in which the conserved motifs PAFLxR for KDO8PS and GARNxQ for DAH7PS feature, is important for the binding of A5P and E4P, respectively. This suggests that subunit packing and interface interactions are tightly coupled with active-site architecture, and hence substrate selection preferences.

Careful comparison of the shared tetrameric structure of KDO8PS and type Iβ DAH7PS reveals some subtle yet potentially important differences in the subunit assembly. Superimposing just the A subunits shows that the remaining subunits of Iβ DAH7PSs are twisted relative to the subunits of KDO8PS (Figure S3, Supporting Information). Focusing on the interface involving the β4-α4 loop shows that the positions of F114R in *Nme*F114R/R117Q and R115 in *Pfu*DAH7PS are essentially identical when just the individual subunits are superimposed (Figure 6). Similarly, the positions of the residues R117Q in *Nme*F114R/R117Q and Gln118 in *Pfu*DAH7PS are very similar (Figure 6). However, the positions of the subunits relative to each other are different. Hence, in *Pfu*DAH7PS, the native Gln (Gln118) is in a different position (the average displacement of the side chain atoms is 4.6 Å), compared to the equivalent R117Q in *Nme*KDO8PS. Thus, although the conserved interface residues in KDO8PS can be converted to the equivalent residues of type Iβ DAH7PSs, unless the relative subunit assembly is also changed, the mutated residues cannot be fulfilling exactly the same roles as in Iβ DAH7PS. The key region for determining relative subunit positioning appears to be the β6-α6 loop, which is in mutual contact among the four subunits. For type Iβ DAH7PS this loop has two residues inserted relative to KDO8PS (Figure S1). This loop for KDO8PS contains a GY motif where the Gly is absolutely conserved. Relative to one subunit, the spatial demands of this loop force a realignment involving rotation and translation of the other subunits of the tetramer, especially the subunits bearing the conserved PAFLxR and GARxN motifs.

■ CONCLUSIONS

The mutations made to the conserved PAFLxR motif of KDO8PS to convert, in part, the β4-α4 active-site loop to the conserved GARNxQ motif found in the evolutionary parent of KDO8PS, illustrate clearly the importance of this motif to KDO8PS function. These mutations did not, however, engender a switch in substrate preference from A5P to E4P. In addition to contributions to the active site, this motif also forms part of an intersubunit interface. Although individual subunits bearing the F114R and R117Q mutations superimpose closely on the corresponding DAH7PS subunit in this region, the subunit interface remains structurally unaltered by the mutations, and the relative positioning of the pair of subunits for either wild-type or mutant KDO8PS enzymes remains significantly different to that observed for type Iβ DAH7PS. Mutations that remove positive charge from the cross over region of this interface have dramatic effects on k_{cat} highlighting a key role of the interdigitating Arg in providing electrostatic guidance to A5P. Moreover, mutations to this β4-α4 loop region that altered positioning of this Arg had disastrous effects on the Michaelis constant for A5P, K_m^{A5P}, and thus on catalytic efficiency k_{cat}/K_m^{A5P}. Somewhat unusually, subtle restructuring of the oligomeric assembly appears to be the key to evolution of KDO8PS from type Iβ DAH7PS.

■ ASSOCIATED CONTENT

Supporting Information

Alignment of KDO8P synthase and DAH7P synthase sequences, the characterization and melt temperatures of wild-type and mutant *Nme*KDO8PS and quaternary structure interactions of *Pfu*DAH7PS compared to the structure of *Nme*F114R/R117Q. This material is available free of charge via the Internet at http://pubs.acs.org.

Accession Codes

The atomic coordinates and structure amplitudes have been deposited with the Protein Data Bank (http://www.rcsb.org/) with the following accession numbers: 4JTE, 4JTF, 4JTG, 4JTH, 4JTI, 4JTJ, and 4JTK.

■ AUTHOR INFORMATION

Corresponding Author

*Telephone (+64) 3 364 5682, Fax (+64) 3 364 2110, E-mail emily.parker@canterbury.ac.nz.

Funding Statement

This research was funded, in part, by the New Zealand Marsden Fund (UOC0710). The College of Science, University of Canterbury provided a Doctoral Scholarship for TMA and the Rigaku MM007/RAxisIV++ X-ray generator and detector was funded by the Allan Wilson Centre for Molecular Ecology and Evolution. The Lottery Health Grants Board of New Zealand for funded the capillary optic at Massey University.

Notes

The authors declare no competing financial interest.

■ ACKNOWLEDGMENTS

Part of this research was undertaken on the MX1 beamline at the Australian Synchrotron, Victoria, Australia.

■ ABBREVIATIONS

A5P, D-arabinose 5-phosphate; *Aae*, *Aquifex aeolicus*; BTP, 1,3-bis[tris(hydroxymethyl)methylamino]propane; DAH7P, 3-deoxy-D-*arabino*-heptulosonate 7-phosphate; DAH7PS, 3-deoxy-D-*arabino*-heptulosonate 7-phosphate synthase; DSF, differential scanning fluorimetry; E4P, D-erythrose 4-phosphate; *Eco*, *Escherichia coli*; IPTG, isopropyl β-D-thiogalactopyranoside; 3-deoxy-D-*manno*-octulosonate 8-phosphate; KDO8PS, 3-deoxy-D-*manno*-octulosonate 8-phosphate synthase; *Nme*, *Neisseria meningitidis*; PEP, phosphoenolpyruvate; R.M.S.D., root-mean-square difference; R5P, D-ribose 5-phosphate

■ REFERENCES

(1) Jensen, R. A., Xie, G., Calhoun, D. H., and Bonner, C. A. (2002) The correct phylogenetic relationship of KdsA (3-deoxy-D-*manno*-octulosonate 8-phosphate synthase) with one of two independently evolved classes of AroA (3-deoxy-D-*arabino*-heptulosonate 7-phosphate synthase). *J. Mol. Evol. 54*, 416−423.

(2) Duewel, H. S., and Woodard, R. W. (2000) A metal bridge between two enzyme families. 3-Deoxy-D-*manno*-octulosonate-8-phosphate synthase from *Aquifex aeolicus* requires a divalent metal for activity. *J. Biol. Chem. 275*, 22824−22831.

(3) Subramaniam, P. S., Xie, G., Xia, T., and Jensen, R. A. (1998) Substrate ambiguity of 3-deoxy-D-*manno*-octulosonate 8-phosphate synthase from *Neisseria gonorrhoeae* in the context of its membership in a protein family containing a subset of 3-deoxy-D-*arabino*-heptulosonate 7-phosphate synthases. *J. Bacteriol. 180*, 119−127.

(4) Birck, M. R., and Woodard, R. W. (2001) *Aquifex aeolicus* 3-deoxy-D-*manno*-2-octulosonic acid 8-phosphate synthase: A new class of KDO 8-P synthase? *J. Mol. Evol. 52*, 205−214.

(5) Bentley, R. (1990) The shikimate pathway - a metabolic tree with many branches. *Crit. Rev. Biochem. Mol. Biol. 25*, 307−384.

(6) Cochrane, F. C., Cookson, T. V. M, Jameson, G. B., and Parker, E. J. (2009) Reversing evolution: Re-establishing obligate metal ion dependence in a metal-independent KDO8P synthase. *J. Mol. Biol. 390*, 646−661.

(7) Wang, J., Duewel, H. S., Woodard, R. W., and Gatti, D. L. (2001) Structures of *Aquifex aeolicus* KDO8P synthase in complex with R5P and PEP, and with a bisubstrate inhibitor: Role of active site water in catalysis. *Biochemistry 40*, 15676−15683.

(8) Duewel, H. S., Radaev, S., Wang, J., Woodard, R. W., and Gatti, D. L. (2001) Substrate and metal complexes of 3-deoxy-D-*manno*-octulosonate-8-phosphate synthase from *Aquifex aeolicus* at 1.9 Å resolution. Implications for the condensation mechanism. *J. Biol. Chem. 276*, 8393−8402.

(9) Shumilin, I. A., Bauerle, R., Wu, J., Woodard, R. W., and Kretsinger, R. H. (2004) Crystal structure of the reaction complex of 3-deoxy-D-*arabino*-heptulosonate-7-phosphate synthase from *Thermotoga maritima* refines the catalytic mechanism and indicates a new mechanism of allosteric regulation. *J. Mol. Biol. 341*, 455−466.

(10) Asojo, O., Friedman, J., Adir, N., Belakhov, V., Shoham, Y., and Baasov, T. (2001) Crystal structures of KDOP synthase in its binary complexes with the substrate phosphoenolpyruvate and with a mechanism-based inhibitor. *Biochemistry 40*, 6326−6334.

(11) Sau, A. K., Li, Z., and Anderson, K. S. (2004) Probing the role of metal ions in the catalysis of *Helicobacter pylori* 3-deoxy-D-*manno*-octulosonate-8-phosphate synthase using a transient kinetic analysis. *J. Biol. Chem. 279*, 15787−15794.

(12) Shulami, S., Yaniv, O., Rabkin, E., Shoham, Y., and Baasov, T. (2003) Cloning, expression, and biochemical characterization of 3-deoxy-D-*manno*-2-octulosonate-8-phosphate (KDO8P) synthase from the hyperthermophilic bacterium *Aquifex pyrophilus*. *Extremophiles 7*, 471−481.

(13) Wu, J., Patel, M. A., Sundaram, A. K., and Woodard, R. W. (2004) Functional and biochemical characterization of a recombinant *Arabidopsis thaliana* 3-deoxy-D-*manno*-octulosonate 8-phosphate synthase. *Biochem. J. 381*, 185−193.

(14) Sheflyan, G. Y., Sundaram, A. K., Taylor, W. P., and Woodard, R. W. (2000) Substrate ambiguity of 3-deoxy-D-*manno*-octulosonate 8-phosphate synthase from *Neisseria gonorrhoeae* revisited. *J. Bacteriol. 182*, 5005−5008.

(15) Kona, F., Xu, X., Martin, P., Kuzmic, P., and Gatti, D. L. (2007) Structural and mechanistic changes along an engineered path from metallo to nonmetallo 3-deoxy-D-*manno*-octulosonate 8-phosphate synthases. *Biochemistry 46*, 4532−4544.

(16) Shulami, S., Furdui, C., Adir, N., Shoham, Y., S., A. K., and Baasov, T. (2004) A reciprocal single mutation affects the metal requirement of 3-deoxy-D-manno-2-octulosonate-8-phosphate (KDO8P) synthases from *Aquifex pyrophilus* and *Escherichia coli*. *J. Biol. Chem. 279*, 45110−45120.

(17) Oliynyk, Z., Briseno-Roa, L., Janowitz, T., Sondergeld, P., and Fersht, A. R. (2004) Designing a metal-binding site in the scaffold of *Escherichia coli* KDO8PS. *Protein Eng. Des. Sel. 17*, 383−390.

(18) Li, J., Wu, J., Fleischhacker, A. S., and Woodard, R. W. (2004) Conversion of *Aquifex aeolicus* 3-deoxy-D-*manno*-octulosonate 8-phosphate synthase, a metalloenzyme, into a nonmetalloenzyme. *J. Am. Chem. Soc. 126*, 7448−7449.

(19) Light, S. H., and Anderson, W. F. (2013) The diversity of allosteric controls at the gateway to aromatic amino acid biosynthesis. *Protein Sci. 22*, 395−404.

(20) Wu, J., and Woodard, R. W. (2006) New insights into the evolutionary links relating to the 3-deoxy-D-*arabino*-heptulosonate 7-phosphate synthase subfamilies. *J. Biol. Chem. 281*, 4042−4048.

(21) Webby, C. J., Jiao, W., Hutton, R. D., Blackmore, N. J., Baker, H. M., Baker, E. N., Jameson, G. B., and Parker, E. J. (2010) Synergistic allostery, a sophisticated regulatory network for the control of aromatic amino acid biosynthesis in *Mycobacterium tuberculosis*. *J. Biol. Chem. 285*, 30567−30576.

(22) Cross, P. J., Dobson, R. C., Patchett, M. L., and Parker, E. J. (2011) Tyrosine latching of a regulatory gate affords allosteric control of aromatic amino acid biosynthesis. *J. Biol. Chem. 286*, 10216−10224.

(23) Kaustov, L., Kababya, S., Du, S., Baasov, T., Gropper, S., Shoham, Y., and Schmidt, A. (2000) Structural and mechanistic investigation of 3-deoxy-D-manno-octulosonate-8-phosphate synthase by solid-state REDOR NMR. *Biochemistry 39*, 14865−14876.

(24) Schofield, L. R., Anderson, B. F., Patchett, M. L., Norris, G. E., Jameson, G. B., and Parker, E. J. (2005) Substrate ambiguity and crystal structure of *Pyrococcus furiosus* 3-deoxy-D-*arabino*-heptulosonate-7-phosphate synthase: An ancestral 3-deoxyald-2-ulosonate-phosphate synthase? *Biochemistry 44*, 11950−11962.

(25) Zhou, L., Wu, J., Janakiraman, V., Shumilin, I. A., Bauerle, R., Kretsinger, R. H., and Woodard, R. W. (2012) Structure and characterization of the 3-deoxy-D-*arabino*-heptulosonate 7-phosphate synthase from *Aeropyrum pernix*. *Bioorg. Chem. 40*, 79−86.

(26) Xu, X., Kona, F., Wang, J., Lu, J., Stemmler, T., and Gatti, D. L. (2005) The catalytic and conformational cycle of *Aquifex aeolicus* KDO8P synthase: Role of the L7 Loop. *Biochemistry 44*, 12434−12444.

(27) Webby, C. J., Baker, H. M., Lott, J. S., Baker, E. N., and Parker, E. J. (2005) The structure of 3-deoxy-D-*arabino*-heptulosonate 7-phosphate synthase from *Mycobacterium tuberculosis* reveals a common catalytic scaffold and ancestry for type I and type II enzymes. *J. Mol. Biol. 354*, 927−939.

(28) Allison, T. M., Hutton, R. D., Jiao, W., Gloyne, B. J., Nimmo, E. B., Jameson, G. B., and Parker, E. J. (2011) An extended β7α7 substrate-binding loop is essential for efficient catalysis by 3-deoxy-D-*manno*-octulosonate 8-phosphate synthase. *Biochemistry 50*, 9318−9327.

(29) Allison, T. M., Hutton, R. D., Cochrane, F. C., Yeoman, J. A., Jameson, G. B., and Parker, E. J. (2011) Targeting the role of a key conserved motif for substrate selection and catalysis by 3-deoxy-D-

manno-octulosonate 8-phosphate synthase. *Biochemistry 50*, 3686−3695.
(30) Allison, T. M., Yeoman, J. A., Hutton, R. D., Cochrane, F. C., Jameson, G. B., and Parker, E. J. (2010) Specificity and mutational analysis of the metal-dependent 3-deoxy-D-*manno*-octulosonate 8-phosphate synthase from *Acidithiobacillus ferrooxidans*. *Biochim. Biophys. Acta, Proteins Proteomics 1804*, 1526−1536.
(31) Ericsson, U. B., Hallberg, B. M., DeTitta, G. T., Dekker, N., and Nordlund, P. (2006) Thermofluor-based high-throughput stability optimization of proteins for structural studies. *Anal. Biochem. 357*, 289−298.
(32) Pflugrath, J. W. (1999) The finer things in X-ray diffraction data collection. *Acta Crystallogr., Sect. D: Biol. Cryst. D55*, 1718−1725.
(33) Bailey, S. (1994) The CCP4 suite: programs for protein crystallography. *Acta Crystallogr., Sect. D: Biol. Cryst. D50*, 760−763.
(34) Murshudov, G. N., Vagin, A. A., and Dodson, E. J. (1997) Refinement of macromolecular structures by the maximum-likelihood method. *Acta Crystallogr., Sect. D: Biol. Cryst. 53*, 240−255.
(35) Emsley, P., and Cowtan, K. (2004) Coot: model-building tools for molecular graphics. *Acta Crystallogr., Sect. D: Biol. Cryst. D60*, 2126−2132.
(36) Ahn, M., Pietersma, A. L., Schofield, L. R., and Parker, E. J. (2005) Mechanistic divergence of two closely related aldol-like enzyme-catalysed reactions. *Org. Biomol. Chem. 3*, 4046−4049.